bio-protocol

Open Access

Published: Jan 05, 2026

A Compact Schlieren Optics Device for Imaging Biological Samples

Yimeng Tong and Jay X. Tang*

Physics Department, Brown University, Providence, RI, USA
*For correspondence: Jay_Tang@Brown.edu

Abstract

Conventional Schlieren optics equipment typically operates on a large optical table, which is inconvenient for imaging small samples or thin layers of transparent materials. We describe an imaging device based on Schlieren optics, aided by a slight shift in light reflected from two surfaces. The device is designed to place the sample between a thick concave mirror and a camera next to a point-light source located at the spherical origin of the concave mirror. The compact device is portable and convenient. It is similarly capable of sensitively detecting patterns in gaseous or liquid media created by a density gradient when the optical effect is too subtle to be detectable by regular cameras and scanners. The new device is particularly suitable for detecting translucent samples, including thin fluid films on the order of micrometers, tissue slices, and other biological samples. We show two examples of how our device can be applied to imaging biological samples. The first compares images acquired using several techniques of a bacterial swarm spread over an agar plate; the second is a set of images of human cells grown on a tissue culture plate.

Key features

- The protocol presents the design of a compact Schlieren optics device (CSOD), with image boundaries enhanced by a slight shift in two overlapping, virtual images.
- The CSOD captures high-resolution images of a transparent medium with variation in thickness or index of refraction.
- The CSOD can detect transparent samples with thickness in the order of 1 μm; it is simple to build, user-friendly, and portable.
- As a cheaper and portable complement to a phase contrast microscope, the device can image large samples more conveniently.

Key words: Schlieren optics, Transparent medium, Density gradient, Thin film, Bacterial colony, Surfactant front

Background

Traditional shadowgraphy is based on the slight shift of rays refracted from a transparent sample. Passing through a transparent medium with a variation in refractive index, such as a stream of gas or compressed air, the light ray is refracted, causing a slight change in direction by an angle [1]. Following the invention of German physicist August Toepler in 1864, a variety of shadowgraph imaging techniques, collectively known as Schlieren optics, have been developed to observe fluid flow by detecting light deflection caused by density gradients that vary the refractive index [2]. Thus, Schlieren optics are widely applied to capture the contours of transparent specimens, including liquids, gases, and air flows [3,4].

Modern Schlieren setups utilize optical components available from global vendors, such as Edmund Optics (https://www.edmundoptics.com). A typical setup involves an optical table, a laser, beam splitters, compound lenses, and a knife-edge strategically and precisely positioned on the optical path. The technique has also been applied in combination with interferometry [5]. A more recent technique, known as the BOS (background-oriented Schlieren) [6], detects fluid non-uniformities by observing the distortion to the image of background grids and is digitally processed to construct the Schlieren image with improved sensitivity.

Although Schlieren systems can effectively identify fluid flow patterns with high sensitivity, they can be affected by disturbances from the transparent medium, such as ambient air, surrounding the test samples [7]. The caveat of large, commercial Schlieren systems is that the light-path distance is rather long [8], especially compared to thin samples of interest. This might explain why we found few previously reported high-quality images on flow patterns of transparent fluids in small liquid volumes (on the order of microliters) or thin layers of fluid, particularly those of biological origin.

Here, we present the design of a compact Schlieren optics device (CSOD). Using a thick concave mirror, we show through optical alignment and calibration that CSOD capitalizes on light's diffraction and interference properties to improve image contrast and sensitivity. We illustrate the usefulness of a simple CSOD in imaging bacterial swarm fronts and clusters of human cells on a culture dish. The simple device described in this protocol may lead to numerous applications, particularly in research involving aqueous, transparent, and biological materials.

Equipment

1. 3D printer with a printing bed larger than 20 × 20 cm (such as an Ender 3s SE)
2. Computer (a PC with Windows 10 version 19041.0 or higher)
3. Soldering iron
4. Screwdrivers (Phillips and Allen)
5. Utility knife
6. Compressed air duster

A. Shopping list

The following is a list of parts, including links to sources for purchase, which we used to construct a CSOD.

1. Camera: https://www.amazon.com/dp/B07CSKXB72
2. Support stand: https://www.amazon.com/dp/B08M37PFQP
3. Mirror: https://www.amazon.com/dp/B079836VBW
4. Lift holder: https://www.amazon.com/dp/B07SX15JHK
5. X-Y stage: https://www.amazon.com/dp/B07VPQT851
6. Power cord: https://www.amazon.com/dp/B0BVBC3DV4
7. Magnet: https://www.amazon.com/dp/B09Y82MTRV
8. 3m screws: https://www.amazon.com/dp/B0BMQ2KJK6
9. 3D printer filament: https://www.amazon.com/dp/B0BV2L2ZTR
10. Camera mount adapter: https://www.amazon.com/dp/B0BNQDWYGW
11. Camera mount conversion mount: https://www.amazon.com/dp/B0CKP2J6XM
12. Camera clamp: https://www.amazon.com/dp/B0CB5JKTBH
13. Led 3 mm: https://www.amazon.com/dp/B077XD19J5
14. Suction cup: https://www.amazon.com/dp/B09BTW2148
15. Solder: https://www.amazon.com/dp/B003X3VUK0

B. 3D-printed parts

1. Adjustment bracket.STL ×1
2. Base adapter.STL ×10
3. Holding rod.STL ×1
4. Lamp rod.STL ×1
5. Mirror arm.STL ×2
6. Nob.STL ×2
7. Rod adapter.STL ×1
8. Sample holding ring.STL ×1
9. Sample rod adapter.STL ×1
10. Slide adapter.STL ×1
11. Top adapter.STL ×1

Software and datasets

1. Windows Camera https://apps.microsoft.com/detail/9wzdncrfjbbg?hl=en-US&gl=US
2. ImageJ (v1.54h) https://imagej.net/ij/download.html

Procedure

A. Overview and assembly

CSOD works in a reflection mode, with an LED light source, a camera, and a sample above a thick concave mirror. Figure 1 shows a picture of the setup with a simplified illustration of the light path next to it. Whereas the majority of light through the sample gets reflected from the bottom mirror surface, a small percentage of light is reflected from the top glass surface of the mirror. Thus, the illumination typically forms two prominent halos as images are captured by the camera.

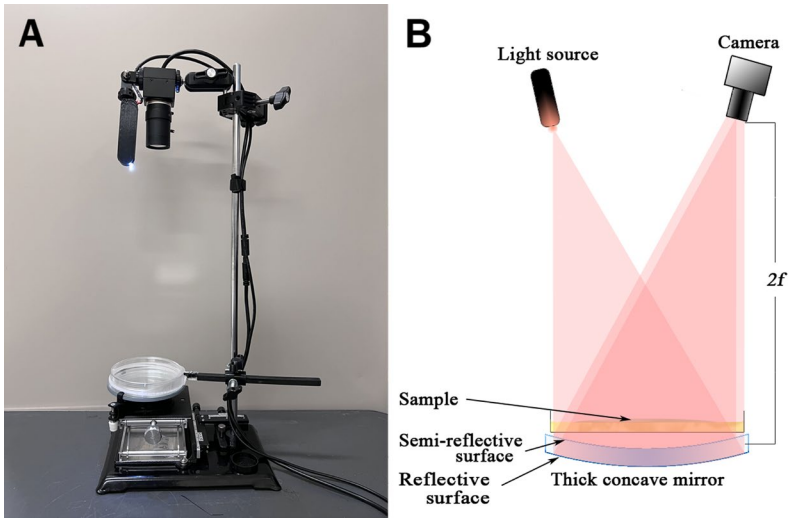

Figure 1. Overview of a compact Schlieren optics device (CSOD). (A) Picture of the device with a sample plate held right above a thick concave mirror with a partially reflective top surface. (B) Diagram illustrating the light path. The camera and the light source are placed on both sides of the mirror's spherical origin. Thus, their vertical distance to the mirror is close to twice the mirror's focal length *f*.

As shown in Figure 2, the CSOD setup consists of four major components: a support stand, a sample holder, a mirror adjustment module, and a camera light source module. The overall assembly of CSOD is as follows:

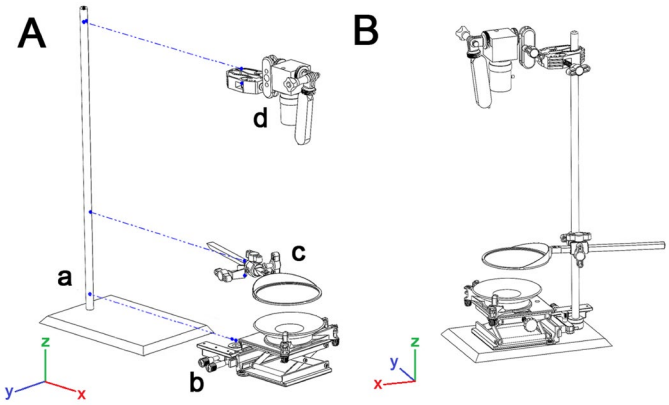

Figure 2. Pictorial assembly instruction for CSOD. (A) The device consists of (a) a lab support stand, (b) a mirror adjustment module, (c) a sample holder, and (d) a camera-light source module. (B) Illustrative drawing of the fully assembled device.

1. Slide the circular loop on the mirror adjustment module down the lab stand's rod until the module magnetically sticks to and aligns with the support stand base.
2. Clamp on the sample holder and the camera-light source module.
3. Adjust the camera lens and light source to be about 30 cm above and point to the center of the thick concave mirror on the mirror adjustment module.
4. Connect the camera and LED lamp from the camera-light source module to a computer using USB cables (not shown) to power them and record images.

B. Mirror adjustment module

The mirror adjustment module consists of a lift assembly, a mirror angle adjuster, a mirror holder, and a concave mirror, as shown in Figure 3.

1. Lift assembly
Note: In Figure 3A, in group (a), the lift assembly has a 3D-printed base adapter (a1) (Base adapter.STL), a 3D-printed top adapter (a3) (Top adapter.STL), a lift stage (a2), two ring magnets (a4), two M3-6 mm screws (a6) with two M3 nuts (a4), and one M5 suction cup bolt (a5). The assembly steps are as follows:
a. Slide the 3D-printed top (a3) and base (a1) adapters onto the lift stage (b2).
b. Screw a ring magnet to the hole on each side of the base adapter (a1) with an M3-6 mm screw (a6) with a nut (a4).
c. Screw the M5 suction cup bolt into the threaded hole on the 3D-printed top adapter (a3).

2. Mirror angle adjuster
Note: In Figure 3A, in group b, the mirror angle adjuster consists of a 3D-printed adjustment bracket (b1) (Adjustment bracket.STL), two 3D-printed knobs (b2) (Nob.STL), two M3-15 mm screws with two M3 nuts (b4), and two 3D-printed mirror arms (b3) (Mirror arm.STL). The assembly steps are as follows:
a. Push each of the M3 nuts into the hexagonal socket on the bottom of each 3D-printed mirror arm.
b. Align the hole of each 3D-printed mirror arm with the slot on each side of the 3D-printed adjustment bracket.
c. Screw an M3-15 mm screw down from the top hole on each side of the 3D-printed adjustment bracket through the aligned hole of the 3D-printed mirror arm with the nut and through the bottom opening on each side of the 3D-printed adjustment bracket.
d. Screw each of the 3D-printed knobs onto the screwed-out portion of the M3-15 mm screw through the bottom opening on each side of the 3D-printed adjustment bracket. Then, turn both 3D-printed knobs to level the mirror arms in the center of the slots on each side of the 3D-printed adjustment bracket.

3. Mirror translation stage
Note: In Figure 3A, in group d, the mirror translation stage includes a 3D-printed rod adapter (d1) (Rod adapter.STL), a microscope X-Y stage (d2), a 3D-printed slide adapter (d3) (Slide adapter.STL), and four M2-4 mm screws (d4). The assembly steps are as follows:

a. Screw the 3D-printed slide adapter onto the microscope X-Y stage using M2-4 mm screws in each of the four holes on the slide that align with the screw holes on the X-Y stage.
b. Fit the 3D-printed rod adapter onto the base of the microscope X-Y stage and tighten them together with the screw knob on the X-Y stage.

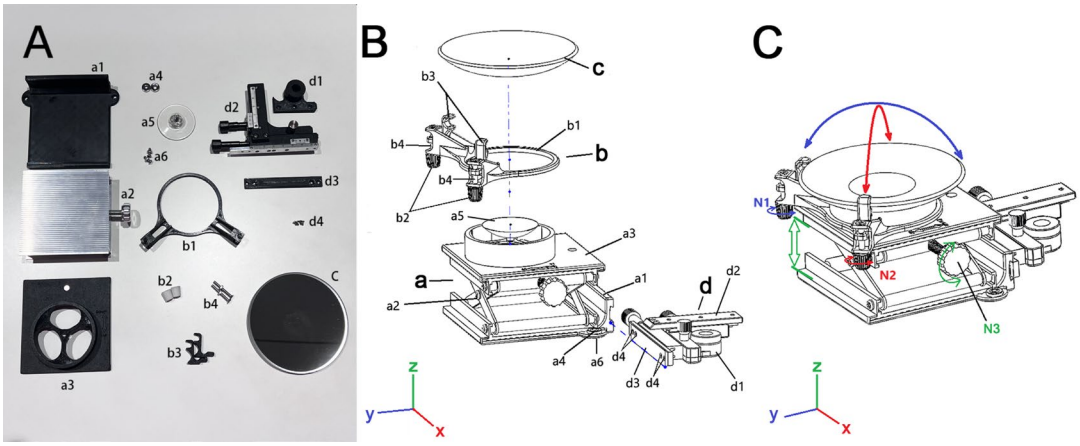

Figure 3. Pictorial instruction for assembling the mirror adjustment module. (A) Components for the mirror adjustment module are grouped as follows: (a) parts for the lift assembly, (b) parts for the mirror angle adjustment, (c) the concave mirror, and (d) parts for the mirror translation stage. (B) Illustration of the mirror adjustment module assembly. (C) Illustration of mirror tilting and lifting adjustment after assembly, with three adjustment knobs noted as N1, N2, and N3.

C. Sample holder module

Note: According to Figure 4, the sample holder module consists of a 3D-printed holding rod (a) (Holding rod.STL), a 3D-printed sample rod adapter (b) (Sample rod adapter.STL), a cross-clamp (c), two M3-8 mm screws (e), one M3 nut (d), a 3D-printed sample holding ring (f) (Sample holding ring.STL), and an adjustment knob (g). The assembly steps are as follows:
1. Attach the 3D-printed sample holding ring to the end of the 3D-printed holding rod using M3-8 mm screws and M3 nuts.
2. Insert the 3D-printed holding rod into the triangular hole of the 3D-printed sample rod adapter and secure it by tightening the adjustment knob screw into the top screw hole of the rod adapter.
3. Secure the 3D-printed sample rod adapter with the horizontal holder of the cross-clamp.

D. Camera-light source module

As shown in Figure 5, the following parts are required for the camera-light source module: a 3D-printed lamp rod (f) (Lamp rod.STL), a DC 5V USB female to male LED strip dimmer switch (k), a camera clamp mount (a), a Sony IMX415 sensor USB camera with a manual 5–50 mm 10× optical zoom lens (b), a 3 mm white LED (j), one 430 Ohm resistor (connected to h), a blue 50 mm breadboard jumper wire with male to female DuPont connectors (h), a red 50 mm breadboard jumper wire with female to female DuPont connector (g), two camera mount adapters (c), a pair of M4 camera thumb bolt nut (e) and screw (d) that came with the mount adapters, one piece of a 20 mm heat shrink tube (i), and a pair of male and female connectors extracted from breadboard jumper wires (connected to k).

The assembly steps are as follows:
1. Secure the USB camera to the clamp mount.
2. Join two camera adapters with the M4 camera thumb bolt nuts and screws to create an elbow joint.
3. Cut the blue DuPont wire in half and insert the 430-Ohm resistor between two sections of the blue wire with a soldering iron and solder.
4. Coat the resistor in the middle of the blue wire with the heat shrink tube and insert the red and blue wire into the 3D-printed lamp rod in the orientation shown in Figure 5B.
5. Insert the 3 mm LED into the female connectors of the blue and red wires, placing the cathode in the socket of the blue wire and the anode in the socket of the red wire.

6. Remove the female USB socket on the USB female to male LED strip dimmer switch, leaving its positive and negative wires exposed. Solder the male DuPont connector to the positive wire and the female DuPont connector on the negative wire.
7. Connect the assembled LED lamp rod with the camera using the elbow joint.
8. Connect the positive wire of the USB dim switch with the red wire on the lamp rod and the negative wire with the blue wire.

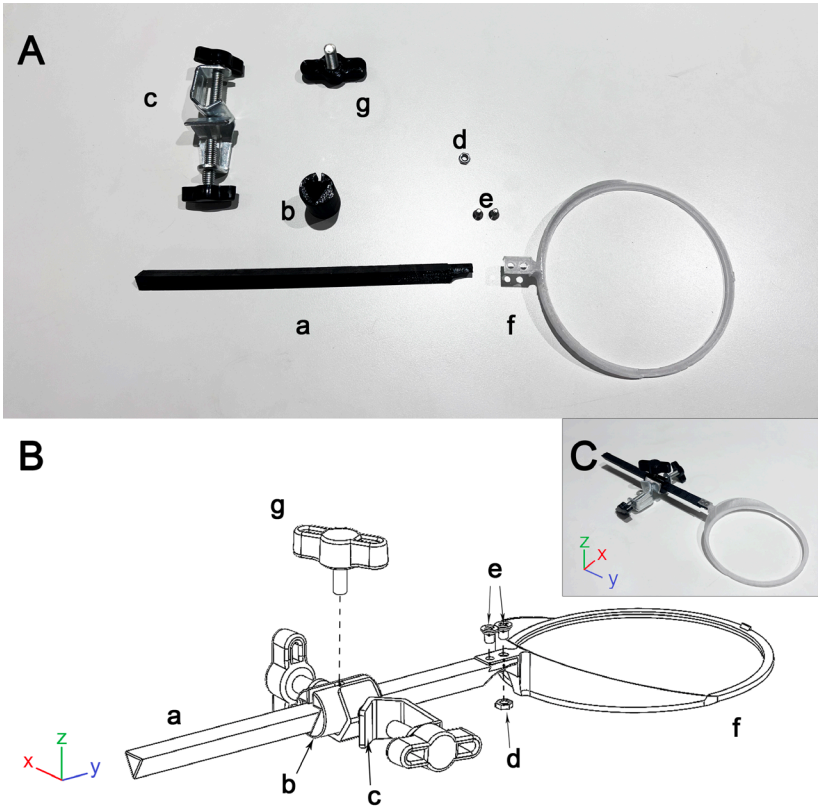

Figure 4. Pictorial instruction for assembling the sample holder. (A) Components for the sample holder, including (a) 3D-printed holding rod, (b) 3D-printed sample rod adapter, (c) cross-clamp, (d) M3 nuts, (e) 8 mm M3 screws, (f) 3D-printed sample holding ring, and (g) adjustment knob. (B) Assembly illustration. (C) Picture of the assembled sample holder.

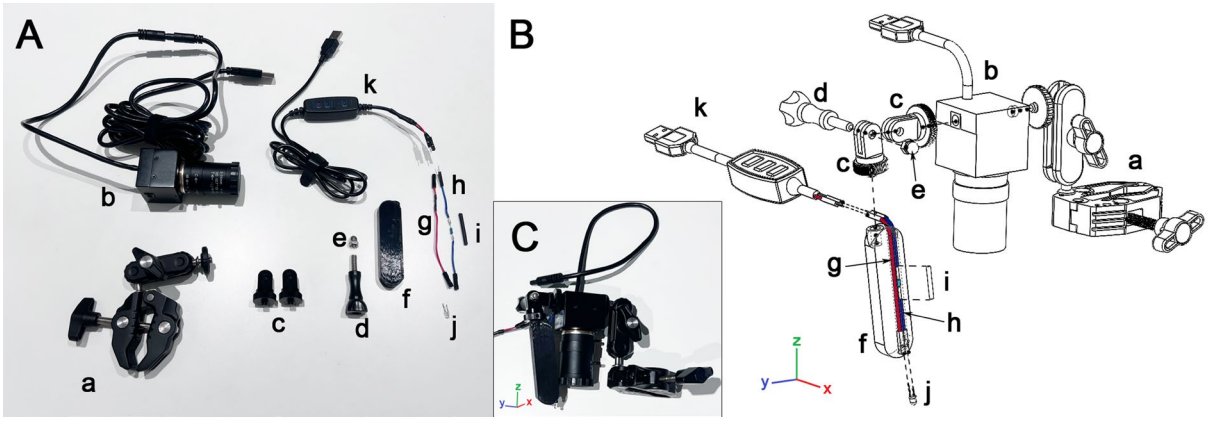

Figure 5. Pictorial instructions for the camera-light source module. (A) Components for the camera-light source module, including (a) camera clamp, (b) USB camera, (c) camera adapter mounts, (d) M5 thumbscrew, (e) M5 acorn nut, (f) 3D-printed lamp rod, (g) red DuPont wire with female to female sockets, (h) blue DuPont wire with male to female sockets and resistor, (i) heat shrink tube, (j) 3 mm LED, and (k) USB dimmer switch with female and male DuPont wire sockets. (B) Assembly illustration. (C) Picture of the assembled module.

E. Device alignment

1. Pre-alignment

A salient feature of CSOD is an enhanced contrast as a result of the slight shift from the overlapping virtual images formed by the two reflective surfaces of the thick mirror. To demonstrate the effect, a stream of compressed air from a straw is readily imaged with the camera and the light source set at the same height, but with a separation distance between 3 and 5 cm. In this pre-alignment setting, the virtual images formed by the two layers of the thick concave mirror are separated, as shown in Figure 6. After passing through the translucent air flow in each virtual image, the reflected light enters the camera lens, forming an image with the air stream casting a shadow. Combining overlapping images from two layers of the concave mirror enhances the visibility of the sample. Although, as noted in Figure 6, each virtual image of airflow is nearly invisible in the center of its own halo, the virtual image formed by rays reflected from the top layer (pink) gains increased contrast when moved into the region of overlap with the more intense reflection from the bottom mirror layer. Therefore, within the overlapped region of the two halos, the airflow stream is clearly visible, with one edge darker and the other edge brighter than the local background. This edge effect is likely due to the refraction of incident light corresponding to the gradient in the air density profile and the slight shift between the two virtual images. Diffraction might also play a role in making the stream of compressed air visible, as it enhances the spatial variation of light intensity at the edges. The effects of diffraction and interference are explored later, with results presented in the supplementary materials.

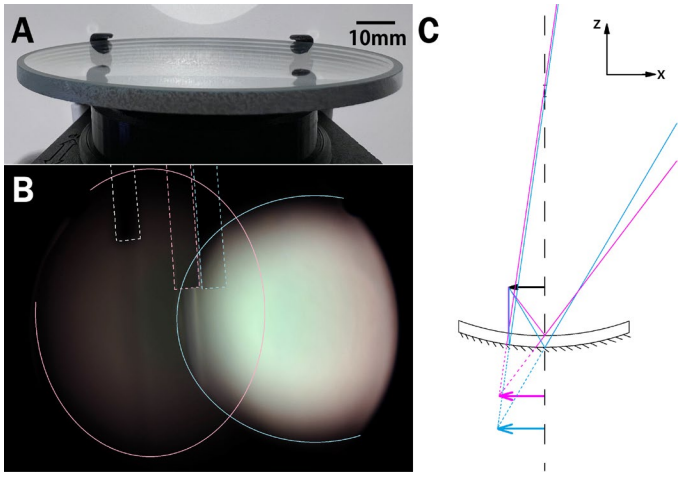

Figure 6. Demonstration of the double shadowing effect in CSOD, along with an illustrative ray diagram. (A) A side-view picture of the thick concave mirror placed on the stage holder. The multiple fringes are due to reflections of the mirror's edge between the top and bottom surfaces of the concave mirror. (B) A combination of shadowgraphs of the duster straw (white dashed rectangle). These halos are the light source reflections created by the two surfaces of the double-layered concave mirror. The halos have different axis orientations, corresponding to the astigmatism of the virtual image, where the light source is placed between the spherical origins for the top and bottom concave mirror surfaces [9]. Note the virtual image of compressed air jetting out in the overlap region of the two halos indicated by the pink and blue elliptical arcs. In contrast, the direct shadow of the air stream from the duster straw, indicated by the white dashed rectangle, is much less visible. The virtual image of the emitted air from the duster straw (blue dashed rectangle) formed by the mirror surface at the bottom is not visible due to the brightness of the halo indicated by the blue arc. (C) A ray diagram locating virtual images of a small object placed close to the concave mirror of two reflective surfaces. The pink and blue arrows indicate virtual images of the duster straw opening, reflected by the top and bottom surfaces of the concave mirror.

2. Alignment

The following steps are taken to align the device:

a Orient and zoom the camera toward the center of the concave mirror while aligning the center of the mirror with the midway point between the camera and the light source from above, using the knobs on the X-Y stage to move the x-axis and y-axis positions of the mirror as shown in Figure 2B.

b. Turn the LED on and adjust the lamp rod so that the distance between the LED and the camera is within about 3 cm, until a pair of the most prominent halos are visible on the computer screen connected to the camera, as shown in Figure 7A. Note a bulge on the larger halo on the right side. It is a higher-order halo due to internal reflections between the two surfaces of the thick mirror (see part B under "General notes and troubleshooting").

c. Adjust the z-knob on the stage to focus on the joint section between the two halos, and use knobs N1 and N2 (see Figure 3C) to adjust the mirror's tilting angle until the halos overlap completely, as shown in Figure 7B and C.
d. The setup is aligned when the reflection halos cover the whole area of the concave mirror, and interference strips form on the mirror and remain stable. These strips are shown in Figure 7C as arcs across the mirror's surface.
e. Blow compressed air over the mirror out of a duster straw. A clear image of the air stream, as shown in Figure 7D, means that the device is fully aligned.

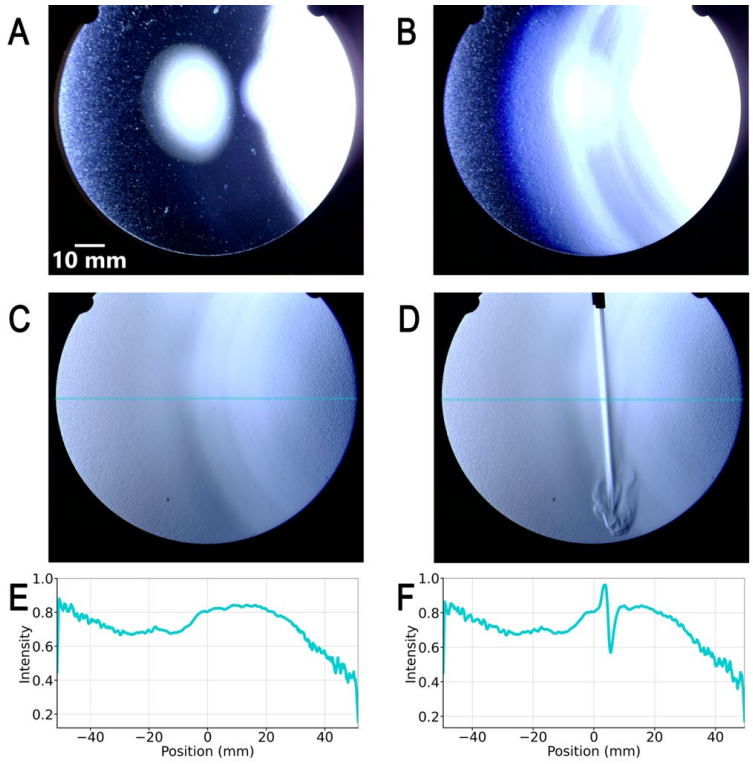

Figure 7. Photos taken from the four alignment steps and intensity profiles corresponding to the last two steps of alignment. (A) Two prominent reflection halos are separated from each other. (B) Interference stripes appear when halos overlap in the mirror center. (C) The centers of the two prominent halos overlap. (D) Compressed air jetting from a duster is visualized near the surface of the mirror. (E) Intensity profile along the line indicated in C. (F) Intensity profile along the line indicated in D. The sharp peak and valley indicate the left and right edges of the air stream, respectively.

F. Operating modes of imaging

Two imaging modes are designed based on the object's position on the optical path. The first position of the object yields a panoramic view of a large sample up to the size of a 10-cm-diameter Petri dish, and the second position produces a magnified image of tunable magnification.

1. Panoramic imaging
The panoramic observation combines real and virtual images. When placing the sample directly on the surface of the concave mirror, as illustrated in Figure 1, the camera captures images of both the object directly and the combination of virtual images formed by the mirror surfaces. The direct image of the object displays the surface features, and the combined virtual image reveals inhomogeneities inside the translucent sample.
The camera lens captures the direct image with the light emitted by the LED reflected by the sample's surface. With a given direction of the incident light emitted from the LED lamp, the reflection rays have a reflection angle equal to the incident angle relative to the sample surface normal. Thus, the reflected light from each point of the sample travels in a different direction because of the slight variation in local orientation or curvature across the sample surface.
In the panoramic observation mode, the sample is placed right above the mirror. The virtual image of the sample lies slightly below the mirror's surface. The camera can detect either the actual sample or—with a slight adjustment—the virtual image of the sample. The light emitted by the LED passes through the sample twice, once before being reflected by the thick

concave mirror and again afterward. When light passes through the sample, obstacles within the medium refract the incoming rays and attenuate the light intensity. The inhomogeneities of the refractive index cause the light passing through each point of the sample to alter its direction of travel.
Panoramic observation simultaneously captures direct and virtual images. For the direct image, the camera captures the image of the sample formed by light reflected off its surface, which reveals its curvature. The complete overlap of two virtual images produced by the top and bottom surfaces of the thick concave mirror results in enhanced contrast, corresponding to the local variation in refractive index due to density variation in the sample. Meanwhile, the shadow cast by the obstacles inside the sample reveals other features that block light.

2. Magnified imaging
A second mode of operation results in a virtual and magnified image. In this mode, the sample is positioned a short distance below the mirror's focal point, as illustrated in Figure 8. The virtual image is magnified and appears significantly below the concave mirror, while the direct image of the sample falls outside the camera's field of vision. The magnification of the virtual image is tunable, as it depends on the relative distance between the sample and the mirror. The exact magnification is calibrated by imaging a transparent ruler, placed at the same location as the sample of interest. The magnified imaging path features a longer light path, enhancing the light's displacement in the horizontal plane while maintaining the same reflective angle. One additional feature of this setting is that the magnified virtual image is actually an overlap of two virtual images formed by reflections from the top and bottom surfaces of the thick concave mirror. Due to a slight shift from perfect overlap, edges of objects are typically highlighted with one side appearing brighter and the opposite side darker. Thus, the combined image reveals fine features due to local variations in refractive index and diffraction of tiny objects and edges.

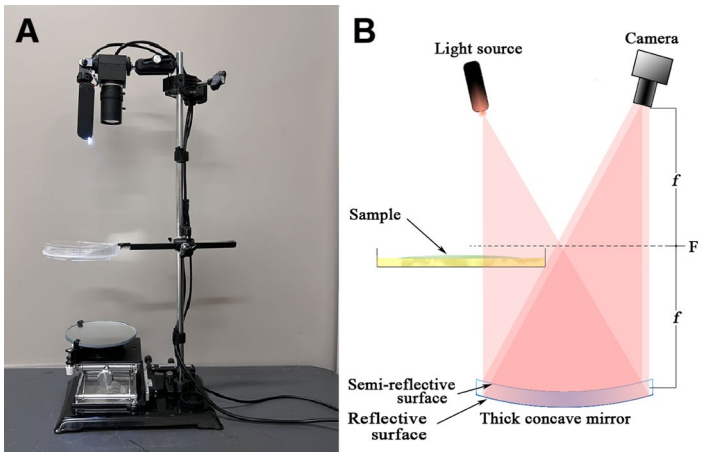

Figure 8. Virtual magnified imaging setup of CSOD. (A) Picture of the device with the sample module placed approximately midway between the light-camera module and the mirror adjustment module. (B) Schematics showing the sample placed slightly below the focal plane, *F*, which is midway between the light source and the mirror surface. The focal length is indicated as *f*. This setting provides a tunable magnification up to 20× of an observational area in the order of 1 m^2.

Data analysis

An example in data analysis is the measurement of the spreading area of a liquid droplet on agar containing mucin, a glycoprotein relevant to human physiology. This has been previously published using an earlier version of our imaging technique [10]. It was a shadowgraph technique, with only the light reflected from the bottom mirror surface captured by the camera. The detailed analysis can be found in the section "Measuring the kinetics of droplet spreading" of our previous publication. Briefly, starting 40 s after droplet deposition, a series of snapshots of the droplet was taken using the magnified imaging method at 10-s intervals, with subsequent images processed by Fiji (ImageJ). Then, a Python script utilizing OpenCV was applied to identify the edges of the circular droplets, resulting in the droplet's radius as a function of time. Such a data analysis procedure applies equally well whether the images are captured by the shadowgraph setup or by CSOD.

Validation of protocol

Our device has been used to image a large swarm of bacteria on an agar plate. The swarming of *P. aeruginosa* on agar plates has been extensively studied, such as in [11,12]. Here, we compared images acquired through the two imaging modes, one through the Foucault knife-edge Schlieren optics, and an image acquired through a scanner.

Compared with a conventional image taken by a scanner [13], as shown in Figure 9A, Schlieren optics images (Figure 9B–D) better resolve the optical inhomogeneities that reflect variations in the density and thickness of the bacterial colony. They also show a transparent fluid-like layer that extends beyond the edge of a bacterial swarm. The front of this liquid-like layer, which is referred to as a surfactant front [13], may alternatively be the edge of a region of slightly thicker gel due to local swelling [14], and is most visible in the image taken using the panoramic mode of CSOD (Figure 9C). A thin fluid layer, which contains a monolayer of bacteria in the swarm front, is also visible under CSOD (Figure 9G) and confirmed by phase-contrast microscopy (Figure 9H–I).

The second example application of our device is to image human cells in a dish, as shown in Figure 10. These human cells on a plate are visible in the region outside the shadow cast by the wall of the cell culture dish. By adjusting the position of the disk, different areas of the plate can be imaged. These images are acquired more conveniently than using an optical microscope equipped with phase contrast, differential interference contrast (DIC), or fluorescence features. Note in the comparison, as shown in Figure 9, that optical microscopy typically yields images of larger magnifications but a narrower field of view.

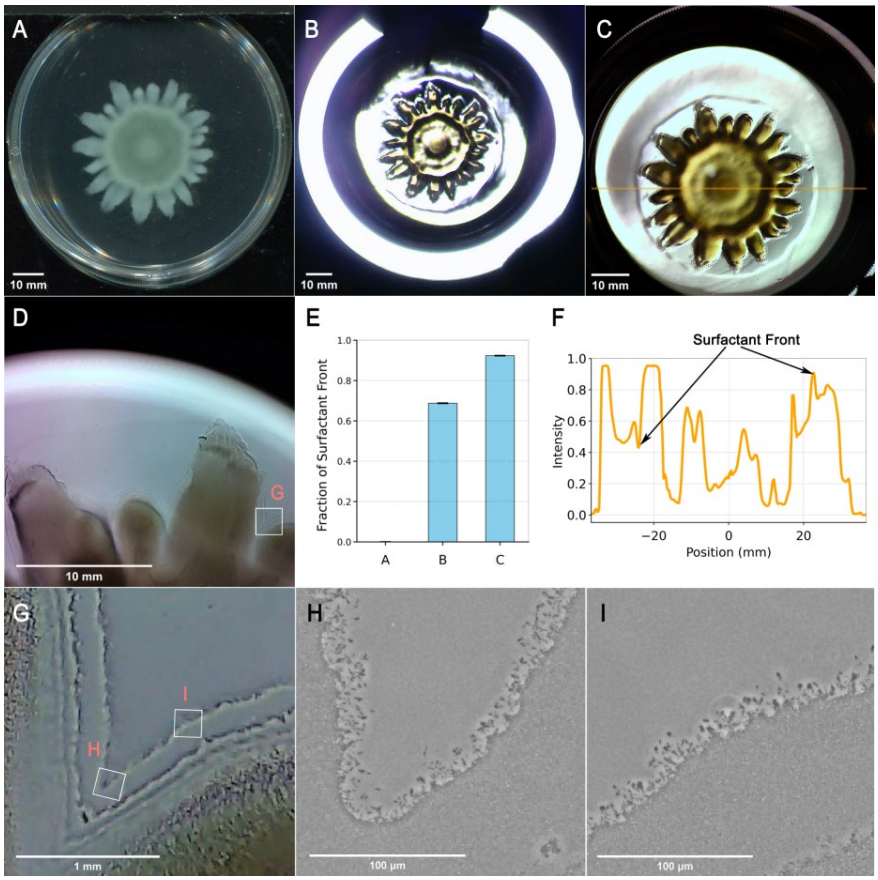

Figure 9. Comparison of images between existing and compact Schlieren optics device (CSOD) techniques. (A) Imaging via an EPSB11B207221-Perfection V370 scanner [13]. (B) Imaging via a Foucault-knife-edge-test Schlieren optics with a light path of 4.0 meters [3]. (C) Imaging via CSOD by panoramic observation, as illustrated in Figure 1. (D) Imaging using the virtual magnifying imaging setup, as illustrated in Figure 8. (E) Comparison of visible surfactant front on images taken by the three techniques, as shown in A–C. (F) Intensity profile of the line scan, as drawn in C. The positions of the surfactant edge on both sides are indicated. (G) Digitally magnified image of the white box in D. (H, I) Images taken using a phase-contrast microscope with a 10× lens. (H) Monolayer of bacteria between two fingers in the region; (I) side of a fingertip with bilayer visible in the lower-right corner.

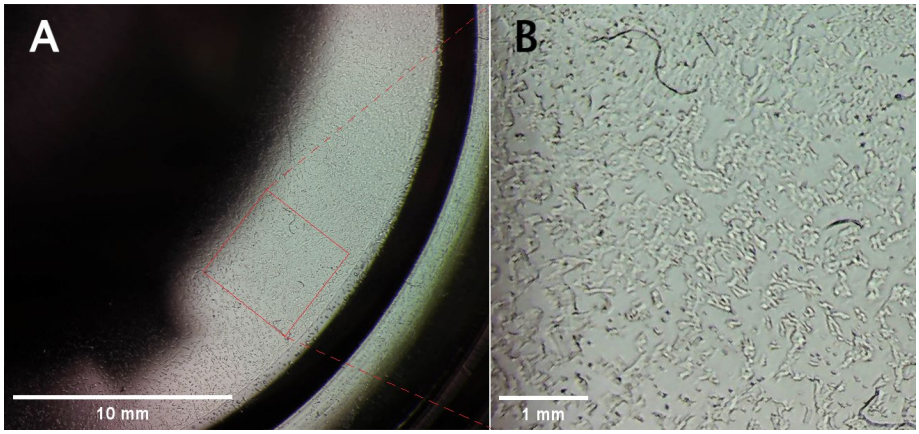

Figure 10. Images of MCF-10A, a type of mammary gland cell, taken via CSOD. (A) Image taken with the virtual magnified image setup, as illustrated in Figure 8. (B) An 8× magnified image, taken with the same setup but with the dish holder moved up to a higher position.

General notes and troubleshooting

A. Selection of mirrors and sample containers

Consideration is required when selecting optical components. First, a single-layer mirror does not produce the Schlieren effect in our CSOD. When the CSOD setup is aligned using a single-layer mirror, neither direct nor virtual images of the compressed airflow can be observed. When the light source's halo covers the entire mirror surface, the intense reflection of the single-layer mirror overwhelms the patterns of the compressed air stream (Figure 11). As a result, the sensitivity of the single-layer mirror is significantly lower than that of the CSOD equipped with a double-layer mirror. In comparison, Figure 7 shows that a stream of compressed air is visible using a double-layer mirror, which proves to be a key feature in the design of our CSOD setup.

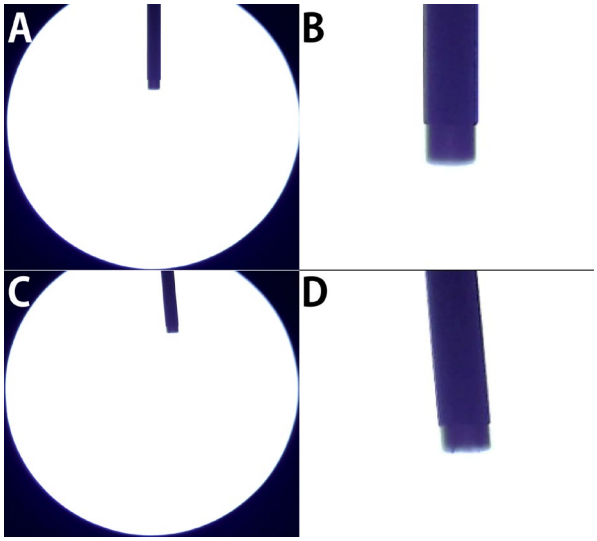

Figure 11. Photos taken from the compact Schlieren optics setup using a single-layer concave mirror of 10 cm focal length. (A) The duster's pipe is placed near the surface of the mirror. (B) Magnified view of the duster pipe tip in panel A. (C) A compressed air stream blowing across the single-layer mirror surface is invisible, other than some minor distortion near the pipe opening. (D) Magnified view of the duster pipe tip in panel C. Note the front edge of the straw head is a bit rougher here than as shown in B, due to local variation in the refractive index caused by the compressed air.

Second, the thick concave mirrors from EISCO Labs (https://www.eiscolabs.com), the particular brand used to build our device, exhibit a slight difference between the curvatures of the upper and lower surfaces, and hence the positions of the two focal points corresponding to the upper and lower surfaces. Such a variation leads to slightly different images from those shown in Figure 7. Due to this variation, researchers may need to purchase multiple mirrors from EISCO Labs or other vendors to select mirrors with desired properties.
Another technical concern is the type of sample container to achieve optimal imaging. For example, an issue was observed when imaging a sample in a tissue culture plate with some obstacles cast as shadows. This limitation was more notable when the device was set up to acquire a magnified virtual image suitable for imaging a relatively small area. As shown in Figure 10A, the thick rim and the rectangular holder of a 50 mm diameter well cell culture plate cast a shadow that covers more than half of the field of view, so only a small area of the plate was imaged. Choosing a culture plate with fewer obstructions can avoid this undesirable effect.

B. High-order reflections and interference strips

Additional optical features are noted during the alignment process, with typical images shown in Figure 7. Before aligning the center line of the mirror with the midpoint between the light source and the camera, as shown in Figure 7A, higher-order reflections occur due to internal reflections of light between the two surfaces of the thick concave mirror. Images that emerge following multiple reflections appear as multiple halos, with higher-order ones increasingly harder to discern. For example, evidence of a secondary image is shown as a bulge at the left edge of the bottom reflection halo. Adjusting the tilt angle of the concave mirror, the alignment brings higher-order reflections of the light source to the camera view. Halos begin to overlap, producing interference strips. The interference strips appear as arcs across the mirror's surface when higher-order halos touch each other, as shown in Figure 7B and C. These strips in the background serve as an indication of successful alignment.

1. Effect of interference created by higher-order reflections

Here, we explore the effect of interference strips in CSOD using a partial alignment setting. In this setting, the distance between the light source and the camera is closer than in Figure 6, but farther than in Figure 7. As shown in Figure 12, the light emitted from the light source creates three prominent halos, two of which are reflections from the top and bottom surfaces of the thick concave mirror. The direct reflection of the light source from the bottom mirror surface is noted as the zeroth-order halo because of its intense brightness. The direct reflection from the top glass surface of the thick mirror forms the first-order halo. The second-order halo is produced by the internal reflection of the zeroth-order reflection at the upper surface of the glass, reflected again by the mirror surface at the bottom, emerging into the space above, and then forming the third halo next to the second one in the image. In this intermediate alignment, the second-order halo is separated from the zeroth-order halo. Interference strips appear when the first-order halo overlaps with the second-order halo. It is interesting to note that in Figure 6, the intersection between the zeroth and first-order halos does not show interference fringes, perhaps due to the huge disparity between their intensities. In short, we note that in this intermediate alignment setting, interference fringes occur between the first-order and the second-order halos, which might be visible because of their comparable intensity.

2. A laser light source reveals the flow field of the compressed air

In fact, finer details of CSOD imaging may be revealed by leveraging the properties of light interference. As shown in Figure 13, we deliberately used a laser as the light source to amplify the effects of interference. We used a 650-nm laser as the light source. With the setup aligned according to the steps in Figure 7, the interference strips cover the entire surface of the double-layer mirror. The stream of compressed air is clearly visible against the background interference fringes. In addition, changes in the refractive index of the surrounding air distort the interference fringes around the jet of compressed air. As a result, the interference stripes are much more prominent so that even the surrounding flow field caused by the compressed air stream becomes visible. This result shows that CSOD can reveal finer details of samples of interest using a laser as a coherent light source.

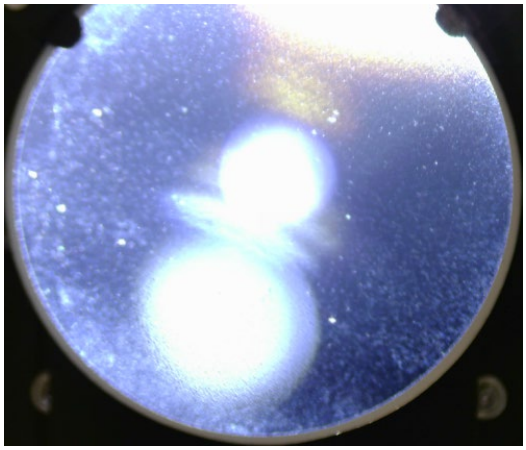

Figure 12. Demonstration of interference strips in CSOD. From top to bottom, the three reflection halos represent the zeroth, second, and first orders of light reflections from the thick concave mirror. The direct reflections from the bottom and top layers correspond to the zeroth-order and the first-order halos. The zeroth-order reflection reflects internally between these layers before re-emerging in air, resulting in the second-order halo. Interference strips occur when the first- and second-order halos overlap near the center of the mirror.

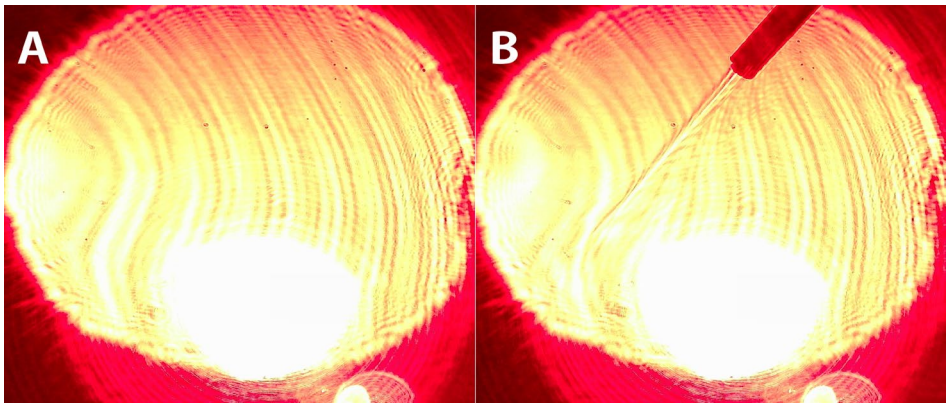

Figure 13. Photos taken from CSOD using a 650 nm laser as its light source. (A) Interference fringes appear when two reflection halos overlap. (B) Visualization of compressed air jetting from a duster. The spread of compressed air surrounding the jet stream is also evident in the distortion of the fringes.

C. Future outlook

CSOD has the potential to be more versatile and advantageous than conventional Schlieren setups. For example, by equipping the system with better optical components and selecting double-layer mirrors with parallel surfaces, researchers could quantitatively calibrate the spatial intensity gradient of the resulting images based on the properties of known samples [15,16]. In addition to the optical design, controlling the degrees of freedom of its components with electronic devices, CSOD can be applied to remote working conditions, such as observing the growth of cells or bacterial colonies inside a sealed incubator. Since the device enables rapid and repeatable imaging, it is also amenable to automated tracking, as well as AI applications in the future.

D. Conclusion

CSOD utilizes overlapping virtual images produced by a double-layer mirror to reveal fine details of transparent materials, including a compressed air stream, features at the air–liquid or liquid–agar interface, bacterial swarm front, and clusters of human cells on a culture dish. Using a shorter light path than its larger traditional counterparts, CSOD can capture high-resolution images of a transparent sample due to variation in density or thickness within the sample. With a light path of

only 30 cm, our design has simplified Schlieren equipment by replacing a set of large components on an optical table into smaller pieces assembled into a compact, portable device.

Acknowledgments

Several members of the Tang biophysics lab at Brown University participated in the experiments, using a previous version of the technique [10]. Most notably, Brandon Pugnet used the current device to acquire images (such as Figure 9C) and provided insightful comments. The authors thank Drs. Jiwon Kim and Hyeontae Jeong of Prof. Ian Wong's lab at Brown University for bringing a dish of mammary gland cells for imaging (Figure 10). One coauthor (YT) benefited from an optics class taught by Prof. Kimani Toussaint, who also suggested improvements on this device. YT also expresses gratitude to his parents for funding his studies and device prototypes. This work received additional funding from NSF DMR 2207284 (JT) and from the National Space Grant College and Fellowship Program Opportunities in NASA STEM -80NSSC20M0053 (JT).
Author contribution: Yimeng Tong conceived and developed the device, generated images, and co-wrote the paper. Jay X. Tang described the optical principles, illustrated the optical path drawing, identified key applications, and co-wrote the paper.

Competing interests

The authors declare that they have no competing interests.

Received: September 08, 2025; Accepted: November 13, 2025; Available online: December 03, 2025; Published: January 05, 2026

References

1. Hargather, M. J. and Settles, G. S. (2012). A comparison of three quantitative schlieren techniques. *Opt Lasers Eng.* 50(1): 8–17. https://doi.org/10.1016/j.optlaseng.2011.05.012
2. Settles, G. and Covert, E. (2002). Schlieren and Shadowgraph Techniques: Visualizing Phenomena in Transport Media. *Appl Mech Rev.* 55(4): B76–B77. https://doi.org/10.1115/1.1483362
3. Settles, G. S. (2018). Smartphone schlieren and shadowgraph imaging. *Opt Lasers Eng.* 104: 9–21. https://doi.org/10.1016/j.optlaseng.2017.07.002
4. Zhou, Z., Wang, H. and Liu, H. (2019). Application of the Quantitative Monochrome Calibrated Schlieren Technique in a Highly Loaded Turbine Cascade Test. *J Turbomach.* 141(11): e4045088. https://doi.org/10.1115/1.4045088
5. Pavez, C., Pedreros, J., Avaria, G., Bora, B., Moreno, J. and Soto, L. (2018). A methodology for the digital reconstruction of an interferogram, a schlieren image, or a shadowgram from a single digital holographic recording. *Rev Sci Instrum.* 89(12): e5023388. https://doi.org/10.1063/1.5023388
6. Shimazaki, T., Ichihara, S. and Tagawa, Y. (2022). Background oriented schlieren technique with fast Fourier demodulation for measuring large density-gradient fields of fluids. *Exp Therm Fluid Sci.* 134: 110598. https://doi.org/10.1016/j.expthermflusci.2022.110598
7. Settles, G. S. and Hargather, M. J. (2017). A review of recent developments in schlieren and shadowgraph techniques. *Meas Sci Technol.* 28(4): 042001. https://doi.org/10.1088/1361-6501/aa5748
8. Auliel, M. I., Hebrero, F. C., Sosa, R. and Artana, G. (2017). Schlieren technique in soap film flows. *Exp Fluids.* 58(5): e1007/s00348–017–2311–4. https://doi.org/10.1007/s00348-017-2311-4
9. Hnilicka, B., Besancon-Voda, A., Schroder, H. J. and Filardi, G. (2002). Modelling the focus error characteristic of a DVD player. *Proc IEEE Int Conf Control Appl.* 2: 629–630. https://doi.org/10.1109/cca.2002.1038672
10. Pawul, C., Dutta, T. T., Johnson, S. G. and Tang, J. X. (2024). Mucin Promotes Bacterial Swarming by Making the Agar Surface More Slippery. *Langmuir.* 40(52): 27307–27313. https://doi.org/10.1021/acs.langmuir.4c03395
11. Yang, A., Tang, W. S., Si, T. and Tang, J. X. (2017). Influence of Physical Effects on the Swarming Motility of Pseudomonas aeruginosa. *Biophys J.* 112(7): 1462–1471. https://doi.org/10.1016/j.bpj.2017.02.019

12. Ma, H., Bell, J., Chen, W., Mani, S. and Tang, J. X. (2021). An expanding bacterial colony forms a depletion zone with growing droplets. *Soft Matter.* 17(8): 2315–2326. https://doi.org/10.1039/d0sm01348j
13. Bru, J. L., Siryaporn, A. and Høyland-Kroghsbo, N. M. (2020). Time-lapse Imaging of Bacterial Swarms and the Collective Stress Response. *J Visualized Exp.* 159: e3791/60915. https://doi.org/10.3791/60915
14. Deforet, M. (2023). Long-range alteration of the physical environment mediates cooperation between *Pseudomonas aeruginosa* swarming colonies. *Environ Microbiol.* 25(8): 1451–1464. https://doi.org/10.1111/1462-2920.16373
15. Gena, A. W., Voelker, C. and Settles, G. S. (2020). Qualitative and quantitative schlieren optical measurement of the human thermal plume. *Indoor Air.* 30(4): 757–766. https://doi.org/10.1111/ina.12674
16. Alvarez-Herrera, C., Moreno-Hernández, D., Barrientos-García, B. and Guerrero-Viramontes, J. (2009). Temperature measurement of air convection using a Schlieren system. *Opt Laser Technol.* 41(3): 233–240. https://doi.org/10.1016/j.optlastec.2008.07.004